Local-field and effective-background effects in coupled integrated photonic waveguide systems

Anastasiia Sheveleva, Mathieu Leonardo, Christophe Finot, and Pierre Colman*
Laboratoire Interdisciplinaire Carnot de Bourgogne UMR CNRS 6303,
Université Bourgogne–Franche-Comté, 9 Avenue Savary, 21000 Dijon, France

(Received 12 August 2022; revised 28 February 2023; accepted 4 May 2023; published 1 June 2023)

The coupling constant between two nearby waveguides is usually predicted using formulas derived from the perturbative theory applied to the electromagnetic Maxwell equations. These formulas, however, fail to provide any reliable estimate when the index contrast between the core of the waveguide and its cladding becomes large. We demonstrate in this paper that a good accuracy can be retrieved if the local field effect is taken into account. Moreover, we show that in case of structured and inhomogeneous cladding, an effective background index must be taken into account so that the local field effect correction remains accurate. This theoretical study is the occasion for physics-oriented discussions regarding the impact of the substrate on the interwaveguide coupling constant.

DOI: 10.1103/PhysRevA.107.063502

I. INTRODUCTION

The fine control of the coupling strength between two nearby optical waveguides is a critical feature in photonics. Regarding applications, optical couplers are, for instance, an essential building block for photonic integrated chips [1–3]. They can be considered as the simplest system of coupled waveguides, yet their thorough comprehension is a first essential step toward the control of much more complex systems like nonlinear waveguide arrays [4–7], the realization of optical analog to quantum effects [8–11], and topological systems [12–14]. Moreover, mode coupling can also be invoked in order to explain mode dispersion [15] and can serve as a strategy for dispersion engineering [16,17]. Consequently, this topic has been at the center of numerous theoretical and experimental investigations. These studies focused either on the effective parameters equations that can be used to describe coupled waveguides [18,19], or on the link between the effective parameters and the waveguide geometry [20,21].

A modern approach consists of describing the dynamics of waveguide arrays in terms of optical supermodes rather than individual waveguides. Because the supermodes are shaped by the intermode coupling constants, their chromatic dispersion will also be related to the latter. In particular, dispersion engineering through mode coupling has already been proved a successful strategy for double-ring resonators [22]. More recently, theoretical works were proposed to combine this type of dispersion engineering with the multimodal nature of waveguide arrays in order to facilitate phase matching during parametric processes [16,17]. These new applications require an acute knowledge of coupled waveguide systems, particularly regarding the chromatic dispersion of the coupling constants, and how the latter could be tuned. Moreover, technology has greatly evolved since the first theory about waveguide arrays: slab waveguides have been replaced gradually by more compact ridge waveguides which exhibit much higher optical confinement. As a result, current formulas developed according to perturbative models now fail when they are applied to these new nanophotonic systems. We will detail throughout this paper how these formulas fail, and how some simple modifications allow retrieving an acceptable accuracy.

II. PERTURBATIVE ELECTROMAGNETIC METHOD IN GUIDED OPTICS

A. Hamiltonian formulation of problems in perturbative photonics

Let us first recall the basis equations, and hypothesis, that lead to the coupling formula usually found in literature [18,19,23,24]:

$$\begin{aligned} \nabla \cdot \varepsilon_0 \varepsilon \boldsymbol{E} = 0 \quad & \nabla \times \boldsymbol{E} = -\mu_0 \frac{\partial \boldsymbol{H}}{\partial t} \\ \nabla \cdot \mu_0 \boldsymbol{H} = 0 \quad & \nabla \times \boldsymbol{H} = \varepsilon \varepsilon_0 \frac{\partial \boldsymbol{E}}{\partial t}. \end{aligned} \tag{1}$$

We can first deduce from the translation invariance along the waveguide direction x that the optical mode can be decomposed as

$$\begin{bmatrix} \boldsymbol{E}(x,y,z,t) \\ \boldsymbol{H}(x,y,z,t) \end{bmatrix} = \begin{bmatrix} \boldsymbol{E}(y,z) \\ \boldsymbol{H}(y,z) \end{bmatrix} e^{i\beta x - i\omega t}. \tag{2}$$

Moreover, the longitudinal components of the field $\{E_x, H_x\}$ can be expressed from its transverse components $\{\boldsymbol{E}_\perp, \boldsymbol{H}_\perp\}$, so that the Maxwell equations Eq. (1) can be expressed using only the latter. After some math, and following the guidelines in Ref. [25], we can define a generalized propagation equation where $|\psi\rangle = [\boldsymbol{E}_\perp(y,z); \boldsymbol{H}_\perp(y,z)]$:

$$\frac{\partial}{\partial x}\hat{B}|\psi\rangle = \imath \frac{\omega}{c}\hat{A}|\psi\rangle. \tag{3}$$

*Corresponding author: pierre.colman@u-bourgogne.fr

The corresponding eigenvalue problem with value β_0 and eigenvector $|\psi_0\rangle = [\boldsymbol{E}_{\perp 0}(y,z); \boldsymbol{H}_{\perp 0}(y,z)]$ is then

$$\beta_0 \hat{B}|\psi_0\rangle = \frac{\omega}{c}\hat{A}|\psi_0\rangle. \tag{4}$$

The Hermitian operators $\hat{A}$ and $\hat{B}$ are

$$\hat{B} = \begin{bmatrix} 0 & -\vec{x}\times \\ \vec{x}\times & 0 \end{bmatrix}$$
$$\hat{A} = \begin{bmatrix} \sqrt{\frac{\varepsilon_0}{\mu_0}}\left[\varepsilon - \frac{c^2}{\omega^2}\nabla_t \times \left\{\vec{x}\cdot\left[\frac{1}{\mu}\vec{x}\cdot(\nabla_t\times)\right]\right\}\right] & 0 \\ 0 & \sqrt{\frac{\mu_0}{\varepsilon_0}}\left[\mu - \frac{c^2}{\omega^2}\nabla_t \times \left\{\vec{x}\cdot\left[\frac{1}{\varepsilon}\vec{x}\cdot(\nabla_t\times)\right]\right\}\right]. \end{bmatrix} \tag{5}$$

Knowing an eigensolution $|\psi_0\rangle$, the corresponding propagation constant β_0 is simply the Rayleigh quotient:

$$\beta_0 = \frac{\omega}{c}\frac{\langle\psi_0|\hat{A}|\psi_0\rangle}{\langle\psi_0|\hat{B}|\psi_0\rangle}. \tag{6}$$

These equations are the starting point to construct a perturbative theory [24–26]. We now consider a system of coupled waveguides, where the second one is considered as a perturbation which modifies the field of the first (and vice versa), resulting in new optical modes $|\psi^{(t)}\rangle$. Using the Hamiltonian formulation developed previously, we separate the parts corresponding to the isolated single waveguide equations $\hat{A}_0$ and its corrections $\Delta\hat{A}$:

$$\beta\hat{B}|\psi^{(t)}\rangle = \frac{\omega}{c}(\hat{A}_0 + \Delta\hat{A})|\psi^{(t)}\rangle. \tag{7}$$

By projecting Eq. (7) on the eigenmodes of the isolated basis, the equation can be further simplified, namely, by exploiting the Hermitian property of $\hat{A}$ and $\hat{B}$. In this case the eigenvalue propagation equation becomes

$$(\beta - \beta_0^{(i)})\langle\psi_0^{(i)}|\hat{B}|\psi^{(t)}\rangle = \frac{\omega}{c}\langle\psi_0^{(i)}|\Delta\hat{A}^{(i)}|\psi^{(t)}\rangle. \tag{8}$$

The index $i = \{1, 2\}$ indicates whether the first or second isolated waveguide is considered. Following the conventional coupled-mode theory [3,18], the eigenmode supported by the waveguide array (with the respective propagation constant β) is then approximated as a combination of the isolated waveguides' modes, hence

$$|\Psi^{(t)}\rangle = (a_1|\psi^{(1)}\rangle + a_2|\psi^{(2)}\rangle)e^{i\beta x}. \tag{9}$$

After substituting $|\Psi^{(t)}\rangle$ to Eq. (8) and rearranging the terms, we obtain the two-unknown set of equations:

$$B^{-1}\begin{bmatrix}\beta - \beta_0^{(1)} & 0 \\ 0 & \beta - \beta_0^{(2)}\end{bmatrix}B\begin{bmatrix}a_1 \\ a_2\end{bmatrix} = \frac{\omega}{c}B^{-1}\Delta A\begin{bmatrix}a_1 \\ a_2\end{bmatrix}, \tag{10}$$

where ΔA, B are matrices with elements expressed as

$$B_{ij} = \iint_S \boldsymbol{x}\cdot(\boldsymbol{E}^{(i)*}\times\boldsymbol{H}^{(j)} - \boldsymbol{H}^{(i)*}\times\boldsymbol{E}^{(j)}) \tag{11}$$

$$\Delta A_{ij} = \sqrt{\frac{\varepsilon_0}{\mu_0}}\iint_S\left[E_x^{(i)*}E_x^{(j)}\frac{\varepsilon_i\Delta\varepsilon_i}{\varepsilon_t} + D_y^{(i)*}D_y^{(j)}\frac{\Delta\varepsilon_i}{\varepsilon_i\varepsilon_j} + E_z^{(i)*}E_z^{(j)}\Delta\varepsilon_i\right]. \tag{12}$$

Here $\boldsymbol{E}(y,z)^{(i)}$ is the eigenfield of the ith waveguide, and ε_i is its dielectric constant. Correspondingly, $\Delta\boldsymbol{\varepsilon}_i$ is a perturbation introduced to the ith waveguide by the other one; $\boldsymbol{\varepsilon}_t = \boldsymbol{\varepsilon}_i + \Delta\boldsymbol{\varepsilon}_i$ is then the total dielectric portrait of the system, varying in the transverse (y,z) plane. If we assume $\beta_0^{(1)} = \beta_0 + \frac{\Delta\beta}{2}$ and $\beta_0^{(2)} = \beta_0 - \frac{\Delta\beta}{2}$, then Eq. (10) turns into

$$(\beta - \beta_0)\begin{bmatrix}a_1 \\ a_2\end{bmatrix} = B^{-1}\left(\frac{\Delta\beta}{2}\begin{bmatrix}-1 & 0 \\ 0 & 1\end{bmatrix}B + \frac{\omega}{c}\Delta A\right)\begin{bmatrix}a_1 \\ a_2\end{bmatrix}. \tag{13}$$

For identical waveguides $\Delta\beta = 0$, Eq. (13) can be further simplified as

$$(\beta - \beta_0)\begin{bmatrix}a_1 \\ a_2\end{bmatrix} = \frac{\omega}{c}B^{-1}\Delta A\begin{bmatrix}a_1 \\ a_2\end{bmatrix}. \tag{14}$$

The case of different waveguides, namely, how the mismatch between the waveguides impacts their effective coupling [27,28], will be discussed further in another article. The $\{i, j\}$ off-diagonal elements correspond to the coupling κ_{ij} between the ith and the jth waveguides. Note that the propagation equation is constructed such that the flux of the Poynting vector $(\langle\Psi|\hat{B}|\Psi\rangle)$ is preserved throughout propagation. If applied to the case of moderate modifications of an isolated waveguide, Eq. (8) produces a good quantitative estimate. In particular, it can cope with moving boundaries and polarization issues in high-index problems [24,26]. More details regarding the underlying mathematics and the corresponding electromagnetic Hamiltonian formulation of such a theory can be found in Ref. [24].

The coupling between two adjacent waveguides is ascribed to the evanescent tail of the optical mode which extends far away from the core region of the waveguide and interacts with the neighboring waveguides. For negligibly overlapping waveguide modes ($B_{ij} = \delta_{ij}$) [19], and neglecting both the longitudinal component of the electric field ($E_x = 0$) and the polarization effects caused by the dielectric interface, Eq. (14) admits a simple analytical form, that is [29],

$$\kappa_{ij} = \frac{\omega\varepsilon_0\iint_S \Delta\boldsymbol{\varepsilon}_i\boldsymbol{E}^{(i)*}\cdot\boldsymbol{E}^{(j)}}{\iint_S \boldsymbol{x}\cdot(\boldsymbol{E}^{(i)*}\times\boldsymbol{H}^{(j)} - \boldsymbol{H}^{(i)*}\times\boldsymbol{E}^{(j)})}. \tag{15}$$

Eq. (15) is identical to the formulation derived in seminal works [19,23,29]. The relative impact of the polarization of the electromagnetic field, including the impact of the longitudinal $\boldsymbol{E}_x$ component [24,30], or the nonorthogonality of the isolated waveguide basis [19,23] ($B_{ij} \neq 0$ for $i \neq j$) result in minor changes (for a proper comparison please refer to Appendix A). Therefore, for sake of clarity, only one of these curves will be used for the figures, and simply labeled as "pre-

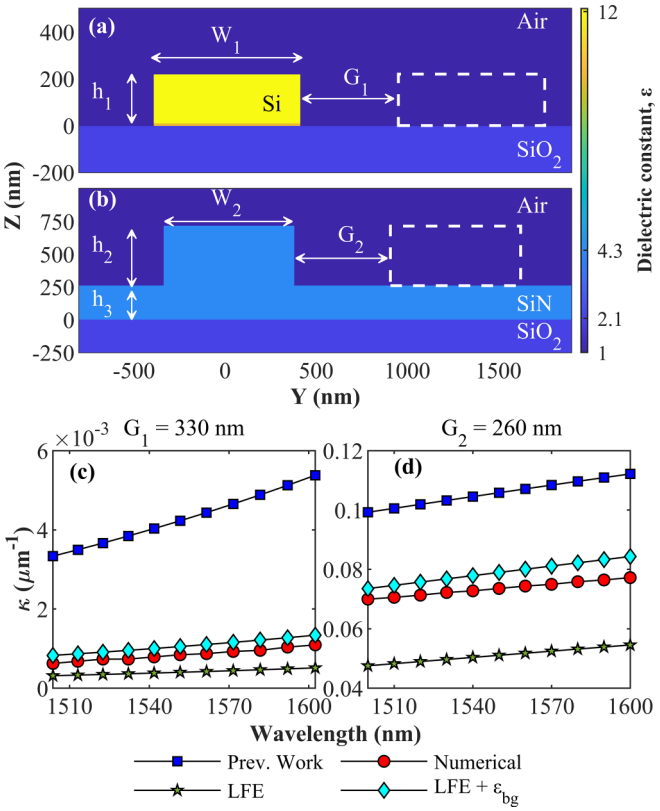

FIG. 1. (a) Dielectric map of the silicon ridge waveguide considered in this work. ($W_1 = 803$ nm, $h_1 = 220$ nm). (b) Dielectric map of the silicon-nitride rib waveguide ($W_2 = 715$ nm, $h_2 = 455$ nm, $h_3 = 260$ nm). (c) Coupling constant κ for two silicon waveguides separated by $G_1 = 330$ nm, as a function of the wavelength. Squares: previous works [18,19,23,24]. Red circles: numerical simulation [37]. Green stars: theory including the local field effect (LFE). Cyan diamonds: theory including the LFE complemented by the concept of the effective background (ε_{bg}). (d) Same as (c), but for the SiN rib waveguides, considering an interwaveguide spacing of $G_2 = 260$ nm.

vious works." As seen in Fig. 5, Eq. (15), or any other similar derivations, actually fail to provide an accurate estimate of the coupling constant (for the high-index contrast systems, as the ones considered in this paper).

B. Coupled waveguide configuration

In order to help the discussion, and provide quantitative information regarding the accuracy of perturbative theory applied to systems of coupled waveguides, we investigate in this article two types of systems that may represent typical situations found in integrated photonics.

First we consider a silicon on insulator coupler [31] composed of two 220-nm-high and 803-nm-wide waveguides [Fig. 1(a)]. This geometry can be considered as a standard in the current integrated photonics industry. It exhibits one of the largest confinements between the core of the waveguide and its cladding. As such, nearly all the light remains confined within the core of the waveguide, and the evanescent tail decays very sharply. This system presents one of the largest index contrasts in dielectric photonics.

The second system under investigation is composed of two silicon-nitride (SiN) rib waveguides [32,33] that are partially etched, leaving out a 260-nm silicon-nitride membrane on insulator [Fig. 1(b)]. The index contrast provided by SiN ($n = 1.6$ up to 2.2) is quite similar to what is found for emerging materials like TiO_2 ($n = 2.5$) [34,35] and Ta_2O_5 [36]. To provide indicative numbers, the contrast between the core of the waveguide and its silica substrate is about $\Delta\varepsilon = 2.4$, nearly 50% smaller than the contrast with the air cladding $\Delta\varepsilon = 3.5$. Moreover, the presence of a high-index thin SiN layer on top of the silica substrate helps extend the evanescent tail of the optical mode farther away from the waveguide. Therefore, despite the index contrast being formally large $\Delta\varepsilon > 1$, the optical mode is actually weakly confined in the core of the waveguide, as is the case for low-contrast systems. Furthermore, we can expect that the properties of this system also depend strongly on the exact structure of the air-SiN-silica stack. This study is thus the occasion to explore the fundamental differences between fully etched and rib waveguides. These systems would constitute a good benchmark to test the robustness and accuracy of perturbative theory in photonics.

In this article the results of Eqs. (14) and (15) are compared against direct simulation of the coupled waveguide system. The electromagnetic field distribution of the isolated waveguides is obtained by simulation using the same plane wave expansion simulation method, namely, the MIT photonics band package (MPB) [37]. Waveguide widths and separations are chosen to match precisely the discretization grid, so as to minimize smoothing errors. Exact parameters used for the MPB simulations, and the relative accuracy of the numerical computation, are presented in Appendix B. Since the chromatic dispersion is mostly dominated in nanophotonics waveguides by the geometry, dispersionless material is assumed.

III. LOCAL FIELD EFFECT

We ascribe the discrepancy in Figs. 1(c) and 1(d) between the numerical simulations and the result of Eq. (11) to the fact that the first-order corrective theory assumes no modifications in the nominal-mode field distribution, despite the introduction of a dielectric perturbation. For large-index contrast systems ($\Delta\varepsilon > 1$), this assumption, however, does not hold because the resulting dipole $\Delta\varepsilon_i \boldsymbol{E}^{(i)}$ created by the dielectric perturbation would then become much larger than the nominal electric field $\boldsymbol{E}^{(i)}$ itself. Therefore, the correction must not be considered as perturbative. Under the influence of the dielectric perturbation $\Delta\varepsilon(r)$, the nominal electric field $\boldsymbol{E}_0$ of an optical mode is modified [38,39]:

$$\boldsymbol{E} = \boldsymbol{E}_0 + \iint_{r\neq r'} \left[\overleftrightarrow{\boldsymbol{G}}_0(\boldsymbol{r},\boldsymbol{r}')k_0^2\Delta\varepsilon(\boldsymbol{r}')\boldsymbol{E}(\boldsymbol{r}')d\boldsymbol{r}'\right] - \frac{L\Delta\varepsilon}{\varepsilon_{bg}}\boldsymbol{E} \tag{16}$$

$\overleftrightarrow{\boldsymbol{G}}_0$ is the Green function (GF) of the unperturbed system [38], and $\boldsymbol{E_0}$ is the unperturbed optical mode. The second term in the right-hand side of Eq. (16) is the well-known contribution of the Green function. The convolution has two major consequences. Firstly, it impacts the electromagnetic fields distribution even outside the region where the dielectric

permittivity is modified. Secondly, the convolution can result in multiple scattering: the resulting optical field does not then solely depend on the dielectric perturbation, but also on the presence of nearby dielectric interfaces. The specificity of the problem considered here is that the optical field propagates in the x direction with a phasor factor (i.e., n_{eff}) that is greater than the nominal dielectric permittivity of the cladding. Consequently, the Green function is of an evanescent nature, hence tightly localized. As a rule of thumb, the decay rate of the GF is of the order of $\alpha = 2\pi/\lambda\sqrt{n_{\text{eff}}^2 - \varepsilon}$, which results in $\alpha = 9.7\,\mu\text{m}^{-1}$ and $\alpha = 6.2\,\mu\text{m}^{-1}$ for the silicon and the silicon nitride waveguides, respectively. Comparing α^{-1} to the characteristic waveguides' widths W and interwaveguide separations G, we can infer that multiple scattering will be a second-order correction in Eq. (16). Therefore, except in the close vicinity of the interface of the dielectric perturbation, the resulting changes in the electric field $\boldsymbol{\Delta E} = \boldsymbol{E} - \boldsymbol{E}_0$ are to a good approximation somewhat proportional to the local averaging of $\boldsymbol{E}$.

The third term in Eq. (16) is called the local field effect (LFE). The origin of the LFE is deeply rooted in the divergence of the Green function in the source region: at this specific location the order of the convolution and of the curl operators cannot be interchanged [40]. When the dielectric background (ε_{bg}) differs from vacuum, it is indeed proved that a correct mathematical derivation results in the correction of the defect polarization $\delta\varepsilon(\vec{r})$ by a dyadic factor $L\Delta\varepsilon\vec{E}(\vec{r})/\varepsilon_{\text{bg}}$ ($L = 1/3$) [40–42]. As we will discuss in more detail later, the L factor depends on the geometry of the problem, namely, the shape of the principal volume, hence the symmetry of the discretization grid. For a general problem computed on a square grid, $L = 1/3$. For other problems, the value of L may change.

In the absence of multiple scattering, and for small-scale perturbations, the LFE contribution dominates. For an homogeneous perturbation over a zone where the electric field varies slowly, a formulation very similar to the LFE can also be derived [41]. The resulting electromagnetic field can then be reasonably approximated as [39]

$$\boldsymbol{E} = \frac{\boldsymbol{E}_0}{1 + \frac{L\Delta\varepsilon}{\varepsilon_{\text{bg}}}}, \tag{17}$$

where ε_{bg} is the background permittivity at the source point. The initial defect polarizability is screened, resulting in a final formula close to the Clausius-Mossotti one [43–45]. However, the physical origins greatly differ. In the case of the Clausisus-Mossotti theory, the reduced apparent polarizability comes from the screening effect that originates from the neighboring dipoles that form an homogeneous polarizable background which counters the initial perturbation. For the LFE, it can be interpreted as the feedback action of a single and isolated dipole on itself, more akin to an impedance mismatch for an antenna: only a small fraction of the polarization defect actually contributes to the modification of the electric field. Even though the resulting effects have similar formulations, and therefore can all be included in the same formula, LFE and screening effects must still be considered as distinct phenomena. Note that the screening action of Eq. (17) would also apply to estimating the defect polarization induced by a dielectric perturbation, which is then not simply $\Delta\varepsilon E_0$ anymore.

The inclusion of the LFE in Eq. (2), is shown in the green-stars line in Figs. 1(c) and 1(d). In brief, the coupled waveguide problem is determined in Eqs. (10)–(14) following the Petrov-Galerkin approach that consists in reducing the dimensionality of the problem by using carefully selected test functions. In particular, the hermiticity of $\hat{A}$ simplifies greatly the resulting problem through the choice of $\langle\psi_0^{(i)}|$ as a test-function basis. This extreme simplification comes at the cost of accuracy. Some precision can then be retrieved through a different choice of the solution functions basis: here Eq. (17) is then injected into Eq. (9). We see that it improves notably the accuracy regarding the silicon waveguide [Fig. 1(c)]. The results are more mitigated for the silicon nitride waveguide on a SiN/SiO_2 substrate [Fig. 1(d)]. The silicon waveguides have the highest index contrast, so that the first-order perturbative theory fails more than for SiN. But in turn the changes in the electric field distribution are much simpler, without long-range contribution of the Green function, and consequently they can be better approximated using the simple formula in Eq. (17).

IV. HIGH-CONTRAST INTEGRATED PHOTONICS

Corrective models of the first order consider small changes to the initial problem. Regarding photonic systems, this implies that the changes $\Delta\varepsilon$ to the nominal dielectric distribution are small enough so that the corresponding defect dipole $\Delta\varepsilon\boldsymbol{E}$ remains much smaller than the nominal optical field $\boldsymbol{E}$. Indeed, any modification of a dielectric interface results in the creation of unphysical free charges if one assumes that the electric field distribution remains unchanged. This issue is as severe as the index contrast is large. As an illustration, two typical examples are presented and discussed in thorough detail in Sec. II B, Figs. 1(c) and 1(d). This typical problem is not surprising, and it can be tracked back to the issue related to the use of an incomplete basis when performing a type of resonant state expansion (RSE) [24,26,46]. Indeed, the perturbative and standard mode expansion methods usually assume that it is possible to describe the modified systems using only the solutions of the unmodified one. However, these few modes are not enough to enforce the divergence free of the electric field in the presence of the large-index contrast dielectric perturbation (namely, the presence of the second waveguide for a coupled waveguide system).

Several strategies can be employed to solve this issue. First, it can be solved by completing the ersatz modes basis with a few unphysical modes that are pure mathematical non-divergence-free solutions of the Helmholtz equation [47,48]. Although this technique results in better numerical accuracy, it does not provide much insight about the actual physics governing the coupled integrated waveguide systems. Another approach would rely on quasi-normal modes (QNMs) [49,50]. For resonant (open) systems, QNMs expansion proves to be quite powerful provided enough modes are accounted for. Hopefully these systems are mostly governed by the resonances with the highest-quality factor so only a few QNMs,

which can be easily identified, are sufficient [51]. For nonresonant systems such as waveguides, however, the choice of the right QNMs might not be straightforward. The possibility offered by this technique will be investigated and discussed in a later study. Finally, the coupling constants could also be retrieved following the analysis of brute force computations of the full system of coupled waveguides [52]. This is usually a simple task on modern computers, but it lacks then any insight regarding the physics governing coupled waveguide systems, so no generalization could be made. The main disadvantage of all these strategies is that they require specific knowledge of the final system, hence the final properties cannot be simply inferred *a priori*. Besides, the large number of modes involved for these accurate modeling complicates the description of the system, hence its design.

The standpoint we chose in this paper is to investigate the first-order models used thus far for describing coupled waveguide systems [19,23]. Indeed, the great advantage of the formulations developed in this context is that they remain simple. All the properties are derived from analytical integral formulas that only require the prior knowledge of general properties of the isolated waveguides, therefore a large variety of configurations can be tested without requiring additional or complex computations. The objective is to extend the current theories past their first-order approximation, in order to improve their accuracy, while preserving their intrinsic simplicity.

The solution we developed here consists in modifying the nominal optical modes so that the mode expansion becomes more accurate, while keeping the required number of modes minimal. This could be achieved by the inclusion of the LFE [40–42] complemented by an effective background theory Figs. 1(c) and 1(d). We rely in particular on the developments that have been recently made regarding disorder in photonics (small perturbations, but high-index contrast) [42,53,54], and demonstrate that they can be extended then to the general case.

V. LFE ON EFFECTIVE BACKGROUND

For better comparison with previous theories, we consider in this article that the individual waveguides only support one single mode, whereas higher-order modes with different polarization actually do exist in integrated waveguides. These restrictions impact the accuracy of the results which we present here, but we believe it allows for a fairer comparison, and also clearer subsequent physics-oriented discussions. Based on the results presented in Fig. 1, taking the LFE into account notably improves the results, but some discrepancies still remain, mostly visible for the silicon nitride waveguides. The remaining error could be partly attributed to an inadequate choice of ε_{air}, resulting in an overestimation of the impact of the LFE. Indeed, the seminal theory of the LFE considers only the case of homogeneous dielectric backgrounds, and in the situation where the perturbation occurs at a dielectric interface, the correct value of the background permittivity is uncertain [42]. Here, while the second waveguide occupies a zone previously filled with air only ($\varepsilon_{\text{air}} = 1$), it is still only a few hundred nanometers away from a higher-index ($\varepsilon_{\text{SiN}} = 4.4$, $\varepsilon_{\text{SiO2}} = 2.3$) substrate. Therefore, it can be expected that the presence of a high-index dielectric interface in the near field of the source region has an impact on its radiation properties [55,56]. Indeed, we checked that, for the case of a waveguide immersed in an homogenous background, the LFE correction results in a more reliable estimation of the coupling constant (Fig. 7). Note that for the silicon waveguides, the index contrasts between the waveguide's core and either the silica substrate or the air cladding are, comparatively, about the same, so that the exact value taken for background permittivity has a lesser influence on the final result.

In its seminal derivation, the LFE is computed for an isolated dielectric perturbation in an infinite and homogeneous background. The dielectric permittivity ε_{bg} stated in the LFE effect is intrinsically linked to the Green function, which is simply related to the homogeneous medium's permittivity. The main difficulty in a practical situation is to adapt the LFE when the presence of either a dielectric inhomogeneity or a structuration notably alters the features of the Green function [57], hence the effective value of $L\varepsilon_{\text{bg}}$ [58]. Considering that the LFE depends on both the local geometry of the problem (for the L value) and the dielectric contrast, this effect can be generalized to the concept of defect polarizability [42], where its impact can be calibrated for a given class of defect. In brief, it consists in fitting the prefactor that would correct the first-order perturbative theory versus the dielectric change $\Delta\varepsilon$, for a given class of problems. The resulting calibration function holds some universality and can then be reused for other perturbative problems of the same class, without requiring complementary *ab initio* simulations. Indeed, the impact of both the geometry, namely, the value of L, and the dielectric structuration, ε_{bg}, are then intrinsically accounted for. This approach has been successfully applied to the investigation of the impact of random imperfections in high-index contrast microphotonic systems such as photonic crystals [42,59]. We demonstrate here that this approach, which has been first developed for small perturbations, remains valid even in the case of an extended perturbation (i.e., waveguides). Furthermore, we focus the discussion on the impact of the local dielectric structuration and show that it has a major impact on the interwaveguide coupling, and that the correct LFE factor can be estimated quite simply [60].

Considering that electromagnetic problems are solved numerically over a finite grid, and that dielectric perturbations are themselves of finite size, the numerical solution of Eq. (16) in the limit of an ultrasmall volume around the source region $\delta_V \to 0$ provides actually the correct solution for the local self-screened response for a dielectric perturbation, including the LFE and other GF-induced scattering [61,62]. At this point, both the LFE and the local screening effect cannot be distinguished anymore from each other [41]. In order to get a better understanding of the role of the substrate, we therefore solved the Green function response to a dielectric perturbation $\Delta\varepsilon$. For generality we consider an $\{x,y\}$ invariant medium where there exists along z an air-dielectric interface, namely, a single air-silica interface for the case of the silicon waveguides, and an air–silicon-nitride–silica interface for the case of the silicon-nitride waveguides. Considering from Eq. (2) that the electromagnetic field propagates with an effective propagation phasor along x $\beta = \frac{\omega}{c} n_{\text{eff}}$, the equation to solve

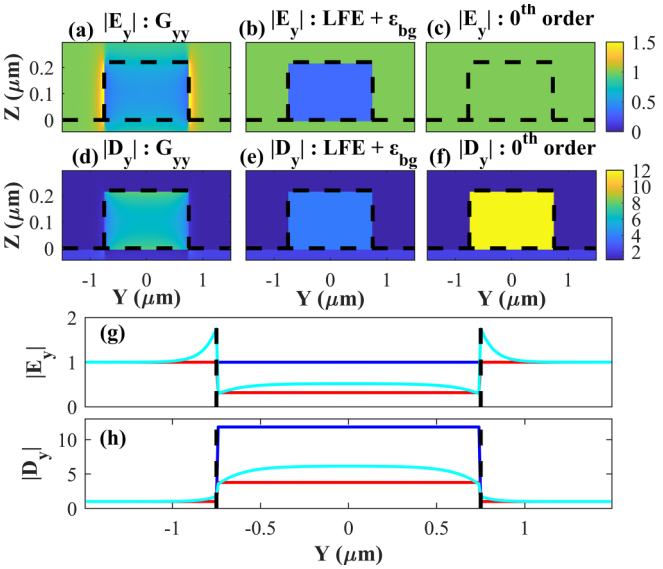

FIG. 2. Case of silicon waveguides. (a–c) y component of the electric field resulting from the perturbation of an initial homogeneous $\boldsymbol{E} = 1\boldsymbol{y}$ field by a dielectric perturbation $\Delta\varepsilon$ which corresponds to the presence of the second waveguide. (a) is the solution of Eq. (16) restricted to the y component of the field. (b) The result of the local field effect assuming an effective background $\varepsilon_{\text{bg}} = 1.7$. (c) Initial coupled mode formulation where no changes of the electric field are assumed (i.e., zeroth-order theory). Black-dashed lines indicate the position of the dielectric perturbation and the limit between the air cladding and the underneath silica substrate. (d–f) y component of the displacement field. (g and h) Variation of the electric field (resp. displacement field) along y, for an altitude of 110 nm (half the waveguide's height). Dark blue: zeroth-order theory (no changes in the nominal electric field). Red: LFE theory assuming an effective background. Light blue: solution of Eq. (18).

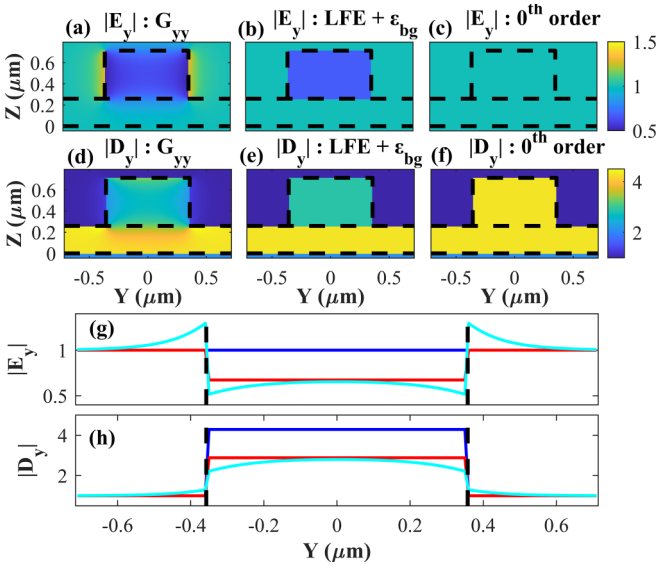

FIG. 3. Case of silicon nitride waveguides. (a–c) y component of the electric field resulting from the perturbation of an initial homogeneous $\boldsymbol{E} = 1\boldsymbol{y}$ field by a dielectric perturbation $\Delta\varepsilon$ which corresponds to the presence of the second waveguide. (a) The solution of Eq. (16) restricted to the y component of the field. (b) The result of the local field effect assuming an effective background $\varepsilon_{\text{bg}} = 2.7$. (c) Initial coupled mode formulation where no changes of the electric field are assumed (i.e., zeroth order theory). Black-dashed lines indicate the position of the dielectric perturbation and the limit between the air cladding and the underneath substrate, which is composed of a thin 260-nm SiN layer on top of a silica substrate. (d–f) y component of the displacement field. (g and h) Variation of the electric field (resp. displacement field) along y, for an altitude of 230 nm (half the waveguide's height). Dark blue: zeroth-order theory (no changes in the nominal electric field). Red: LFE theory assuming an effective background. Light blue: solution of Eq. (18).

is

$$\nabla\times\nabla\times\overleftrightarrow{\boldsymbol{G}}_0 + 2\imath\frac{\omega}{c}n_{\text{eff}}\vec{x}\times(\nabla\times\overleftrightarrow{\boldsymbol{G}}_0) + \left(\frac{\omega}{c}\right)^2 n_{\text{eff}}^2\vec{x}\cdot(\vec{x}\cdot\overleftrightarrow{\boldsymbol{G}}_0) + \left(\frac{\omega}{c}\right)^2\left[\varepsilon(y,z) - n_{\text{eff}}^2\right]\overleftrightarrow{\boldsymbol{G}}_0 = \overleftrightarrow{\delta}(y-y_0, z-z_0). \tag{18}$$

The important point about the problem considered here is that $[\varepsilon(y,z) - n_{\text{eff}}^2] < 0$ at the position of the perturbation. Therefore, the GF solution of Eq. (18) is not a propagating wave but an evanescent-decaying, hence tightly localized, function. This behavior limits strongly multiple scattering. It also strongly alleviates the problems related to the finite size of the simulation domain. We solved Eq. (18) using the Fourier modal expansion (grid size of 10 nm) assuming an unperturbed uniform electric field purely y-polarized $\boldsymbol{E}_0 = 1\vec{y}$. Indeed, the mode field distributions of the waveguide modes considered here are y polarized to about 90%. Thus, these simplifications are still retaining the important features of the initial problem, while allowing a simpler discussion and computation [61,62]. The result for the case of the silicon waveguide is shown in Figs. 2(a) and 2(d).

In contrast to the approximation of the first-order perturbation theory which assumes no modifications in the electric field Figs. 2(c) and 2(f), the new displacement field D_y that is obtained by changing the mode basis in Eq. (9) is now divergence free, as seen in Fig. 2(h). A strong modification ($\Delta\varepsilon > 1$) results in a corresponding decrease of the total electric field in order to minimize discontinuity of the displacement field [Fig. 2(a)]. This retroaction effect is therefore as severe as $\Delta\varepsilon$ is large. Looking in more detail, we observe that the residual discontinuity is compensated by a gradient located at the edges of the dielectric perturbation. The restriction of the changes of the electric field to a generalized LFE cannot take into account these gradients. The LFE complemented by the concept of effective background appears in Figs. 2(b) and 2(e) as a crude approximation of the exact field. Note that the accuracy of the LFE approximation might be directly related to the evanescent nature of the perturbation problem outside the waveguide's core region: multiscattering can be neglected provided the waveguides are not too close to each other. Regarding the silicon-nitride waveguides, the corresponding comparison is shown in Fig. 3.

Whereas solving Eq. (16) assuming a purely y-polarized field worked well for the silicon case, this approximation is a bit worse for the SiN configuration. Its accuracy actually directly depends on the strength of the longitudinal electric field [30]. It illustrates the complexity introduced by the structured

substrate, namely, the presence of a thin SiN layer, compared to a cladding of low refractive index.

The critical approximation that is made about the evaluation of Eq. (16) is the absence of standing waves between the dielectric perturbation and the initial waveguide [18]. The conclusions we draw are then very general: it involves only the structure of the substrate, but disregards subtle effects that would occur at precise interwaveguide separations. In particular, this approximation does not hold for ultra-small-gap separations where the system then becomes a slotted photonic structure which localizes a large portion of its electric field precisely inside the gap. Regarding the subsequent derivation of the LFE [Eq. (17)], the main simplification resides in the absence of a field gradient close to the dielectric interface. That said, the resulting improvement can still be clearly observed in Fig. 1.

VI. EFFECTIVE BACKGROUND

As a result, the key point of the LFE concerns the evaluation of the effective background permittivity ε_{bg}. The value of ε_{bg} in Eq. (17) can be chosen as the fitting parameter that matches best the result of Eq. (16). It only depends on the dielectric configuration of the cladding and substrate. Thus, it can be calibrated for a given technology. Note that for an uniform dielectric cladding, ε_{bg} is simply the latter permittivity, as stated by the nominal LFE derivation (this is illustrated further in Fig. 7). Similarly, the value of ε_{bg} does not depend on the size of the dielectric perturbation, the gradient features set aside. Interestingly, this value can actually be well approximated as the average permittivity felt by the optical mode away from the waveguide's core: $\varepsilon_{bg} = \int \varepsilon(r)|\boldsymbol{E}|^2 / \int |\boldsymbol{E}|^2$. Consequently, if the concept of the effective background permittivity can appear so far as a mathematical fitting parameter, we demonstrate next that it is uniquely defined, and that it is deeply rooted to the optical mode features.

Indeed, let us consider how the coupling constant evolves with increasing interwaveguide spacing. It evolves similarly as the evanescent tail of the optical mode decays away from the waveguide. Therefore, if the mode propagates according to the effective index n_{eff}, then the coupling constant must decay with a rate $\alpha = k_0\sqrt{n_{eff}^2 - \varepsilon_{bg}}$ where k_0 is the vacuum wave vector. Thus, knowing the coupling constant for one interwaveguide spacing, its values at other separation distances can be easily extrapolated.

We see that assuming the nominal vacuum's permittivity [$\varepsilon_{bg} = 1$, blue squares in Fig. 4(b)] results in a large overestimation of the decay rate. This is no surprise because the optical mode decays both in the cladding and in the substrate, and energy can be exchanged between these two media. As a result, the actual decay rate is somehow a mixture of the cladding's and the substrate's rates. However, if one considers now the effective permittivity as the one just defined previously [$\varepsilon_{bg} = 2.7$, cyan diamonds in Fig. 4(b)], the nominal decay factor now matches the numerical simulation. Regarding the silicon ridge waveguide [Fig. 4(a)], the effective index is much larger than the background permittivity so that small changes in the value of ε_{bg} have a much lesser impact than for SiN—and lower indices—waveguides.

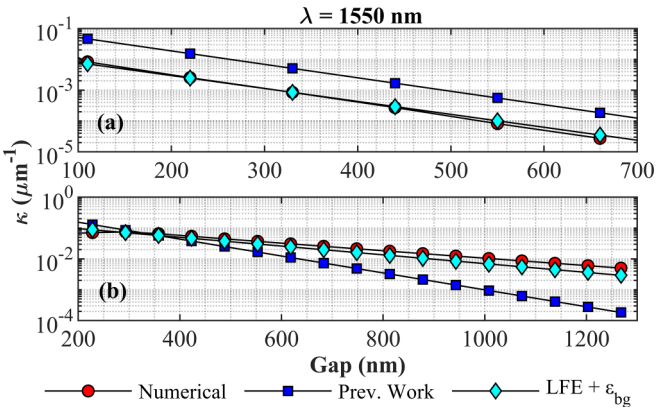

FIG. 4. (a and b) Evolution of the coupling constant κ as function of the interwaveguide spacing (gap). The results obtained from perturbation theories for a gap of 300 nm are assumed to vary with a decay rate $\alpha = k_0\sqrt{n_{eff}^2 - \varepsilon_{bg}}$. Red circles: results from direct simulations. Blue squares: previous perturbative theory where ε_{bg} is assumed to be equal to the cladding permittivity, namely, $\varepsilon_{bg} = \varepsilon_{air} = 1$. Cyan diamonds: new formulation considering an effective background. (a) Case of silicon waveguides, $\varepsilon_{bg} = 1.7$. (b) Case of silicon nitride waveguides, $\varepsilon_{bg} = 2.7$.

From this analysis, we can conclude that the effective background that we introduced is involved both in the LFE and in the natural decay of the optical mode away from the waveguide's core. It is actually no surprise that the optical mode and its associated Green function share some properties. Indeed, according to the Kirchhoff theory, the decaying tail of the optical mode can be interpreted as the propagation—controlled by the Green function—of light from the waveguide's core, which serves as the source. The value of ε_{bg} is then uniquely defined, and therefore must also be considered as a fundamental property of the optical mode, like, for instance, its effective index n_{eff}.

If the complex numerical developments made in Sec. V are essential in order to demonstrate formally that the concept of effective background permittivity is fully justified, and thus does not have arbitrary and convenient fitting parameters, we would like to insist on the fact that reliable estimate of ε_{bg} can be accessed by looking simply at the field decay of the optical mode. In this prospect, even though the coupling for one specific interwaveguide spacing can be estimated more accurately using direct simulation than the current analytical approach, we believe it is also equally important to have a reliable model to extrapolate the coupling at different spacing, being aware that ε_{bg} might not equal the nominal cladding index. This is particularly essential for large waveguide separations where the coupling may be too small to be computed accurately, and therefore is often extrapolated from values measured at smaller separations.

VII. LIMITS AND PERSPECTIVES OF THE PERTURBATIVE APPROACH FOR COUPLED WAVEGUIDES

Compared to the models used previously, the local field effect, complemented by the concept of effective background, improves the estimation of the coupling constant by nearly

an order of magnitude. That said, as seen in Figs. 1(c) and 1(d), some errors still remain. If usually the discrepancy is blamed indistinctively on the high index contrast, we can be a bit more specific here. Note that the specificity of the SiN waveguide systems comes from its index contrast, which is of intermediate value. Indeed, the index contrast is strong enough ($\Delta\varepsilon = 3.29$) to result in a strong confinement, but it is still weak enough so that the exponential tail extends over a very long range ($k_0\sqrt{n_{\text{eff}}^2 - \varepsilon_{\text{bg}}} = 3.4\,\mu\text{m}^{-1}$). This sensibility would make SiN a platform of choice for coupled waveguides and sensing applications. However, the final properties of this type of system are then much harder to infer using a simple analytical formula.

Regarding the rib and ridges waveguides investigated in this paper, the main source of errors for previous analytical formulations clearly comes from the local field effect, which was never considered. Next comes the definition of the effective background, which helps to further improve the accuracy in case of complex substrate or cladding. Other limitations may mainly come from the presence of higher-order modes. For the sake of simplicity, and to allow a fairer comparison with previous works, the waveguides are supposed here to possess only a single guided mode. Actually, integrated waveguides support higher-order modes, and modes of different polarization. These modes are orthogonal by construction, but the presence of a second waveguide, acting as a perturbation, can couple them. This effect is strong as the modes have a similar propagation constant, so it has a great impact on systems with either rotational symmetry (polarization degeneracy) or very large waveguides (small intermode spacing). In principle, Eq. (9) and Eq. (8) can be extended to include the impact of other modes. Note that the presence of angled dielectric interfaces results in further mixing between TE (transverse electric, i.e. mainly E_y polarized mode) and TM (transverse magnetic, i.e. mainly E_z polarized mode) polarized modes. Our choice of square waveguides with a high form factor minimizes the impact of other modes and polarization effects, so that the LFE is singled out. In the most general case, the relative impact of the LFE might be partly screened by multimodal and polarization effects.

In any case, the LFE is always present. Eventually its magnitude may vary depending on the local geometry, as has been demonstrated previously [42]. Its magnitude is directly related to the ratio between the index contrast and the initial permittivity at the position of the perturbation, according to Eq. (17). Consequently, a change of the permittivity by $\Delta\varepsilon \approx 0.3\varepsilon_{\text{bg}}$ would result in a correction of the coupling coefficient by about 10%. Considering the others effects at play in coupled waveguide systems (higher-order modes, polarization, multiscattering properties of the GF, etc.), this could be considered as about the limit where LFE must be taken into account. An important point is that the LFE is dissymmetric depending on whether the perturbation consists of a dielectric addition on a low-index background, or a dielectric subtraction on a high-index material. Conversely, we see that the modification of the core of a waveguide would have a reduced LFE contribution, compared to a modification of its cladding. When it comes to ultrasmall waveguide separations, or the design of slotted waveguides, the right strategy would then be to consider a large initial waveguide whose center has been etched, rather than to use the two-coupled-waveguide description. As practical design rules, especially regarding perturbative—or even mode expansion—theories, the key point is to start with the initial structure which is the closest to the final one.

If the present article focuses on the local field effect, the approach we followed in order to develop the coupled equations may differ from what is usually found in literature (which usually relies on the Helmholtz equation). If all these methods result in about the same analytical expression for the coupling constant Eq. (15) (assuming weak contrast and identical waveguides), they rely on different approximations. Therefore, it could also be interesting to assess how our approach may remain suitable for systems other than the one presented here. First, we demonstrate in Appendix D that Eq. (13) remains valid also for periodic waveguides, such as photonic crystal waveguides. The matrix elements keep the same expression as defined in Eq. (12), the integral over the surface simply becoming an integral over the volume of the unit cell. Note that considering the specific characteristic of the periodic systems, where the frequency ω is usually expressed as a function of the wave vector β_b, the formulation of the eigenproblem in terms of ω rather than β could be more appropriate.

Secondly, the derivation of any coupled-modes equation involves a few assumptions at some point. In this regard we warn the reader to be cautious when applying ready-made formula, like Eq. (15), to other systems. In particular, the formula presented in this article assumes an Hermitian evolution of a well-defined, normalized, nonleaky optical mode. Future work shall focus on leaky and non-Hermitian systems. This is where numerous new applications and innovative strategies are developed, and therefore where having an analytical model to understand these systems could be of great interest. As a typical example, we discuss the strategy that consists in the use of gratings (leaky modes) as a multiplexer to couple distant plasmonics (non-Hermitian) waveguides [63]. If a complete case study exceeds the scope of the present article, we can still provide some indications about how such a system must be taken into account by the coupled mode theory. The passage from Eq. (7) to Eq. (8) requires that $\langle\psi_0^{(i)}|$ is the eigenmode of $\hat{A}^*$. Therefore, in case $\hat{A}$ is not Hermitian, $\langle\psi_0^{(i)}|$ must be replaced by $\langle\psi_0^{(i)\dagger}|$, which is the solution of the adjoint operator. Throughout this article, the operator $\hat{B}$ serves as a normalization factor: it can be interpreted as a direct application of the Lorentz reciprocity theorem. For leaky modes, as found on gratings, modes are then quasi-normal modes [64], and the ortho-normalization procedure must then be changed accordingly [65,66]. This usually consists in using the nonconjugated form of the Lorentz reciprocity theorem.

VIII. CONCLUSION

We demonstrated that the LFE is an important feature in semiconductor integrated photonics, where contrast indices are large. We also showed the importance of the concept of the effective dielectric background ε_{bg} which is involved in both the description of the field decay and the LFE contribution. We managed to derive a simple analytical formula an order of magnitude more accurate than previous developments found

in literature. This study was also the occasion to draw the limits of this analytical approach to describe coupled waveguide systems. These limitations are particularly stringent for high-contrast ($\Delta\varepsilon > 1$) but low-decay ($\sqrt{n_{\text{eff}}^2 - \varepsilon_{\text{bg}}} \leqslant 1$) systems, which include precisely a class of emerging materials (e.g., TiO_2, Ta_2O_5) for photonic integrated chips. If one can argue that with modern computing capabilities, the exact coupling constants can be computed in a timely manner, our study has nevertheless some profound implications. First it demonstrates the impact of the interplay between the cladding and the (structured) substrate on the optical mode properties. This reinforces our vision that a structured substrate forming a metamaterial [67] can be of great importance to tune further the optical properties of integrated photonic circuits. Secondly, if the current development would require some small adjustments of its parameters in order to match exactly the numerical simulation, it nevertheless takes into account the physics of the systems as precisely as possible. In particular, the effective background provides the correct model for the decay of the coupling with increasing interwaveguide separation. Moreover, the chromatic dispersion due to the waveguide's geometry is also now much better described. Therefore, it is possible to infer more precisely how the coupling features are *a priori* impacted by any change in the nominal parameters like, for instance, deriving the wavelength dependence of the coupling constant. The key advantage of the development that we propose here is that it allows to construct at minimal computational cost a test-function basis [or projection basis, Eq. (8)] as complete—or realistic—as possible. Such a strategy has already been permitted to accelerate rigorous coupled-wave analysis algorithms [68]. Finally, by proving the suitability of the LFE concept even in the case of extended defects, this study is also of importance for, and can be extended to, any other systems requiring approximate solutions in photonics at minimal computation cost. Indeed, the LFE allows a first estimation of the modification induced by a dielectric perturbation on the electric field. In particular, optimization methods based on gradient computation [69] could greatly benefit from the LFE.

ACKNOWLEDGMENT

This work was supported by the Agence Nationale de la Recherche (ANR) project "NAC-NIP" (Contract No. ANR-20-CE24-0007).

The authors declare no conflicts of interest.

APPENDIX A: PREVIOUS WORKS

The data in Figs. 1(c) and 1(d) labeled as "Previous works" can be separated into three methods: data obtained from a simplified approach [Eq. (15)] [18,19], perturbative method [Eq. (10)] with longitudinal field included [23], and perturbative method with $\boldsymbol{E}_x$ and $\boldsymbol{E}_y \to \frac{\boldsymbol{D}_y}{\boldsymbol{\varepsilon}}$ (black line, yellow diamonds, and blue circles in Fig. 5, respectively) [24]. The presented methods result in approximately the same results, and they deviate substantially from the results of direct simulations.

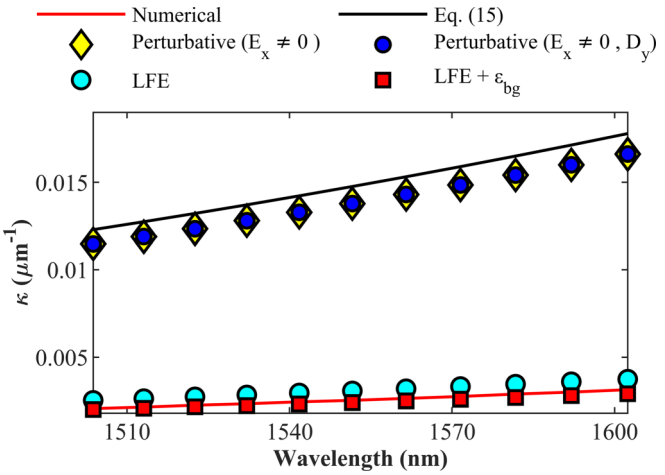

FIG. 5. Coupling constant κ for two silicon waveguides separated by $G_1 = 220\,\text{nm}$, as a function of the wavelength. Red line: numerical simulation. Black line: simplified analytical, from Eq. (15). Yellow diamonds: coupling constant resulting from the perturbative method [Eq. (10)] with longitudinal field $\boldsymbol{E}_x$ included. Dark blue circles: same as previous but continuity of y field is preserved. Cyan circles: theory including the LFE. Red squares: theory including the LFE complemented by the concept of the effective background (ε_{bg}).

APPENDIX B: SIMULATION PARAMETERS (MPB)

Simulations are carried out using the MPB package [37].

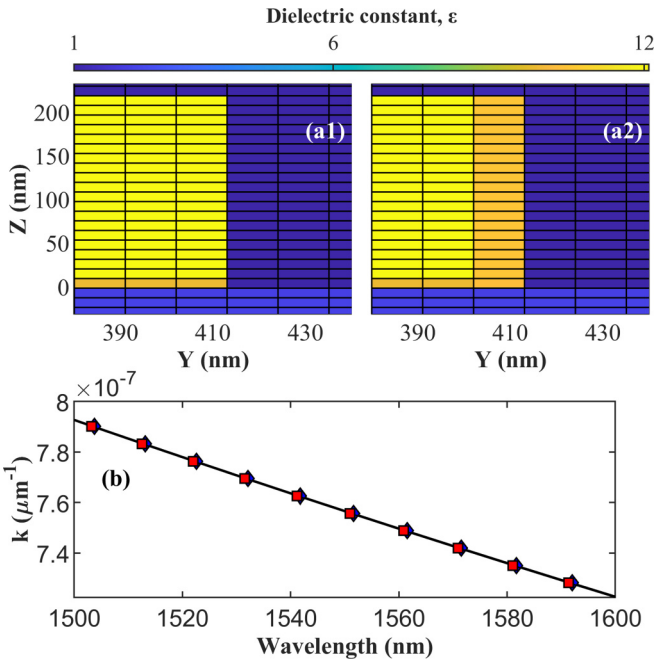

FIG. 6. (log-scale) Absolute error on the coupling constant κ, for silicon waveguides separated by $G_1 = 330\,\text{nm}$, depending on the grid resolution used for the simulation. Dark blue diamonds: situation when the grid is not properly aligned on the waveguides, which creates some smoothing of the dielectric interface. Red square: resolution chosen for this article (40 pixel μm^{-1}).

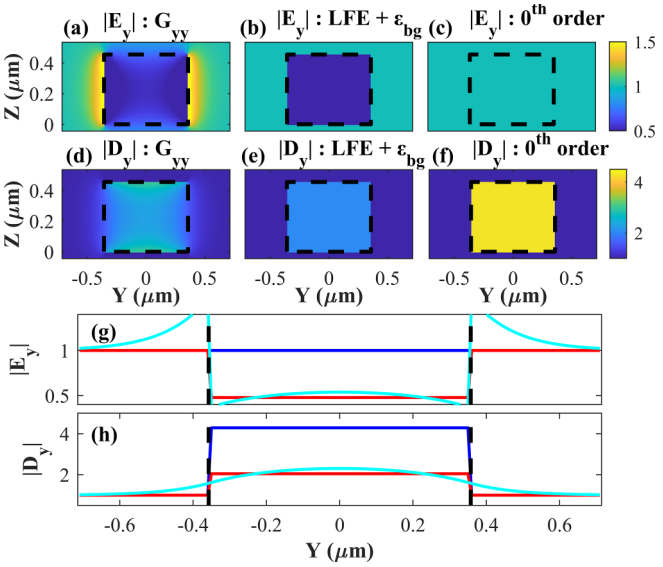

FIG. 7. Case of silicon nitride waveguides in air cladding, $\varepsilon_{\text{bg}} = 1$. (a–c) y component of the electric field resulting from the perturbation of an initial homogeneous $E_y = 1$ field by a dielectric perturbation $\Delta\varepsilon$ which corresponds to the presence of the second waveguide. (a) The solution of Eq. (16) restricted to the y component of the field. (b) The result of the local field effect assuming an effective background $\varepsilon_{\text{bg}} = \varepsilon_{\text{air}} = 1.00$. (c) Initial coupled mode formulation where no changes of the electric field are assumed (i.e., zeroth-order theory). Black-dashed lines indicate the position of the dielectric perturbation and the limit with the air cladding. (d–f) y component of the displacement field. (g and h) Variation of the electric field (resp. displacement field) along y, for an altitude of 230 nm (half the waveguide's height). Dark blue: zeroth-order theory (no changes in the nominal electric field). Red: LFE theory assuming an effective background. Light blue: solution of Eq. (18).

For Si waveguides we have used the following parameters: Global scaling factor of $a = 440$ nm, pixel size 11 nm pixel^{-1}, mesh size 12, resolution 40, tolerance 10^{-9}, range of eigenvalues $k = [0.57{:}1.1334]$ (normalized in $2\pi\ a^{-1}$ unit), simulation geometry width = 24, height = 12 (in a units).

For SiN waveguides we have used the following parameters: Global scaling factor of $a = 650$ nm; pixel size 65 nm pixel^{-1}; mesh size 12; resolution 40; tolerance 10^{-9}; range of eigenvalues $k = [0.5871{:}0.8890]$ (normalized in $2\pi\ a^{-1}$ unit); simulation geometry width = 18, height = 10 (in a units).

Convergence is shown in Fig. 6 for the silicon waveguide (interwaveguide spacing $G_1 = 330$ nm): the coupling coefficient κ is computed with a relative precision of about 2.6%. The accuracy is absolute, so it impacts less the SiN waveguides which have a strong evanescent field, and more situations with large interwaveguide distance. In this regard, this shows that it is also equally important to have a reliable model to describe the evolution of the coupling constant with the interwaveguide spacing. Indeed, weak coupling situations may not be computed accurately, or at huge computational cost. The simulation parameters and the waveguide dimensions are selected to match exactly a discretization grid. Indeed, the MPB package assumes square pixels, therefore the features that do not match the grid exactly would be smoothed, leading to a deviation from the assumed dielectric profile as shown on the blue diamonds in Fig. 6, where an increase of the inaccuracy by 25% is reported. These discrepancies will impact the eigenvalues and hence the accuracy regarding the coupling constant. To minimize the impact of the discretization, rectangular waveguides must be considered.

APPENDIX C: LFE: CASE OF HOMOGENEOUS BACKGROUND

We present in Fig. 7 the analog of Fig. 2 in the case of an homogeneous air-cladding medium. This shows that when the cladding surrounding of the waveguide is composed of an uniform material, then ε_{bg} indeed matches the nominal permittivity of the cladding.

APPENDIX D: PERIODIC SYSTEMS: BLOCH-FLOQUET MODES FORMULATION

We show here that the formulas expressed in Eqs. (13)–(15) remain valid for periodic waveguides subject to the integral over the surface being substituted by a volume integral over the single periodic cell.

The Bloch-Floquet theorem states that the a-periodic systems support eigenmodes that are a-periodic, to a phasor called the Bloch wave vector; hence,

$$\begin{bmatrix}\boldsymbol{E}(x,y,z,t)\\ \boldsymbol{H}(x,y,z,t)\end{bmatrix} = \begin{bmatrix}\boldsymbol{u_E}(x,y,z)\\ \boldsymbol{u_H}(x,y,z)\end{bmatrix} e^{i\beta_b x - i\omega t}, \tag{D1}$$

where $\boldsymbol{u_E}(x,y,z)$ and $\boldsymbol{u_H}(x,y,z)$ are a-periodic, hence $\boldsymbol{u}(x+a,y,z) = \boldsymbol{u}(x,y,z)$. As a consequence, the optical modes are not invariant by ∂_x derivation.

$$\frac{\partial}{\partial x}|\psi\rangle = \imath\beta_b|\psi\rangle + \begin{bmatrix}\partial_x \boldsymbol{u_E}(x,y,z)\\ \partial_x \boldsymbol{u_H}(x,y,z)\end{bmatrix} e^{\imath\beta_b x - \imath\omega t}. \tag{D2}$$

Let now compute the $\{i,j\}$ matrix elements associated to Eq. (3), corresponding to the equivalent of Eq. (8) for periodic structures.

$$\langle\psi_0^{(i)}|\frac{\partial}{\partial x}\hat{B}|\psi^{(j)}\rangle = \iint_S \left(\imath\beta_b\left[\boldsymbol{u_E^{(i)*}}, \boldsymbol{u_H^{(i)*}}\right]\hat{B}\begin{bmatrix}\boldsymbol{u_E^{(j)}}\\ \boldsymbol{u_H^{(j)}}\end{bmatrix} + \left[\boldsymbol{u_E^{(i)*}}, \boldsymbol{u_H^{(i)*}}\right]\hat{B}\begin{bmatrix}\boldsymbol{\partial_x u_E^{(j)}}\\ \boldsymbol{\partial_x u_H^{(j)}}\end{bmatrix}\right) e^{\imath(\beta_b - \beta_b^{(i)})x} \tag{D3}$$

$$\begin{aligned}\imath\frac{\omega}{c}\langle\psi_0^{(i)}|\hat{A}|\psi^{(j)}\rangle &= \imath\frac{\omega}{c}\iint_S \left[\boldsymbol{u_E^{(i)*}}, \boldsymbol{u_H^{(i)*}}\right]\hat{A}\begin{bmatrix}\boldsymbol{u_E^{(j)}}\\ \boldsymbol{u_H^{(j)}}\end{bmatrix} e^{\imath(\beta_b - \beta_b^{(i)})x}\\ &= \imath\frac{\omega}{c}\iint_S \left(\left[\boldsymbol{u_E^{(i)*}}, \boldsymbol{u_H^{(i)*}}\right]\hat{A}^{(i)}\begin{bmatrix}\boldsymbol{u_E^{(j)}}\\ \boldsymbol{u_H^{(j)}}\end{bmatrix} + \left[\boldsymbol{u_E^{(i)*}}, \boldsymbol{u_H^{(i)*}}\right]\Delta\hat{A}^{(i)}\begin{bmatrix}\boldsymbol{u_E^{(j)}}\\ \boldsymbol{u_H^{(j)}}\end{bmatrix}\right) e^{\imath(\beta_b - \beta_b^{(i)})x}\end{aligned} \tag{D4}$$

$$= \iint_S \left(\imath \beta_b^{(i)} \left[\boldsymbol{u}_E^{(i)*}, \boldsymbol{u}_H^{(i)*} \right] \hat{B} \begin{bmatrix} \boldsymbol{u}_E^{(j)} \\ \boldsymbol{u}_H^{(j)} \end{bmatrix} - \left[\partial_x \boldsymbol{u}_E^{(i)*}, \partial_x \boldsymbol{u}_H^{(i)*} \right] \hat{B} \begin{bmatrix} \boldsymbol{u}_E^{(j)} \\ \boldsymbol{u}_H^{(j)} \end{bmatrix} + \imath \frac{\omega}{c} \left[\boldsymbol{u}_E^{(i)*}, \boldsymbol{u}_H^{(i)*} \right] \Delta \hat{A}^{(i)*} \begin{bmatrix} \boldsymbol{u}_E^{(j)} \\ \boldsymbol{u}_H^{(j)} \end{bmatrix} \right) e^{\imath (\beta_b - \beta_b^{(i)}) x}. \tag{D5}$$

The operator $\hat{A}$ has been decomposed into $\hat{A} = \hat{A}^{(i)} + \Delta \hat{A}^{(i)}$. Transforming Eqs. (D4) and (D5) relies on the fact that $|\psi^{(i)}\rangle$ is the solution of the adjoint equation to Eq. (3), hence

$$\frac{\partial}{\partial x} \hat{B} |\psi\rangle = \imath \frac{\omega}{c} \hat{A}^{(i)*} |\psi\rangle. \tag{D6}$$

The periodic nature of $\boldsymbol{u}$ can be put to use by integrating Eqs. (D4) and (D5) along x over a periodic unit cell. In such a case, we have indeed the identity

$$\begin{aligned} \int_{x=0}^{a} \left[\partial_x \boldsymbol{u}_E^{(i)*}, \partial_x \boldsymbol{u}_H^{(i)*} \right] \hat{B} \begin{bmatrix} \boldsymbol{u}_E^{(j)} \\ \boldsymbol{u}_H^{(j)} \end{bmatrix} &= \left[\left[\boldsymbol{u}_E^{(i)*}, \boldsymbol{u}_H^{(i)*} \right] \hat{B} \begin{bmatrix} \boldsymbol{u}_E^{(j)} \\ \boldsymbol{u}_H^{(j)} \end{bmatrix} \right]_{x=0}^{a} - \int_{x=0}^{a} \left[\boldsymbol{u}_E^{(i)*}, \boldsymbol{u}_H^{(i)*} \right] \hat{B} \begin{bmatrix} \partial_x \boldsymbol{u}_E^{(j)} \\ \partial_x \boldsymbol{u}_H^{(j)} \end{bmatrix} \\ &= - \int_{x=0}^{a} \left[\boldsymbol{u}_E^{(i)*}, \boldsymbol{u}_H^{(i)*} \right] \hat{B} \begin{bmatrix} \partial_x \boldsymbol{u}_E^{(j)} \\ \partial_x \boldsymbol{u}_H^{(j)} \end{bmatrix}. \end{aligned} \tag{D7}$$

Dropping the common phasor term $\exp \imath (\beta_b - \beta_b^{(i)}) x$ in Eq. (D3) and Eq. (D5), and integrating these two equations over a unit cell along x results finally after some simplifications in

$$\imath \beta_b \iiint_V \left[\boldsymbol{u}_E^{(i)*}, \boldsymbol{u}_H^{(i)*} \right] \hat{B} \begin{bmatrix} \boldsymbol{u}_E^{(j)} \\ \boldsymbol{u}_H^{(j)} \end{bmatrix} = \imath \beta_b^{(i)} \iiint_V \left[\boldsymbol{u}_E^{(i)*}, \boldsymbol{u}_H^{(i)*} \right] \hat{B} \begin{bmatrix} \boldsymbol{u}_E^{(j)} \\ \boldsymbol{u}_H^{(j)} \end{bmatrix} + \imath \frac{\omega}{c} \left[\boldsymbol{u}_E^{(i)*}, \boldsymbol{u}_H^{(i)*} \right] \Delta \hat{A}^{(i)*} \begin{bmatrix} \boldsymbol{u}_E^{(j)} \\ \boldsymbol{u}_H^{(j)} \end{bmatrix}. \tag{D8}$$

Consequently, if we redefine the scalar product between two terms as the integral over the unit cell of their respective periodic parts ($\{\boldsymbol{u}_E, \boldsymbol{u}_H\}$ instead of $\{\boldsymbol{E}, \boldsymbol{H}\}$), Eq. (D8) can be rewritten as

$$\left(\beta_b - \beta_b^{(i)} \right) \left\langle \psi_0^{(i)} \middle| \hat{B} \middle| \psi^{(j)} \right\rangle = \frac{\omega}{c} \left\langle \psi_0^{(i)} \middle| \Delta \hat{A}^{(i)} \middle| \psi^{(j)} \right\rangle, \tag{D9}$$

which is exactly the matrix elements associated to Eq. (8). If the Bloch-Floquet modes are not strictly eigensolutions of Eq. (3), the perturbative problem can still be put into a set of equations that has exactly the same formulation as Eq. (13).

[1] N. C. Harris, J. Carolan, D. Bunandar, M. Prabhu, M. Hochberg, T. Baehr-Jones, M. L. Fanto, A. M. Smith, C. C. Tison, P. M. Alsing, and D. Englund, Linear programmable nanophotonic processors, Optica **5**, 1623 (2018).

[2] X. Yi, T. X. H. Huang, and R. Minasian, Tunable and reconfigurable photonic signal processor with programmable all-optical complex coefficients, IEEE Trans. Microwave Theory Tech. **58**, 3088 (2010).

[3] W.-P. Huang, Coupled-mode theory for optical waveguides: An overview, J. Opt. Soc. Am. A **11**, 963 (1994).

[4] A. Yulin, D. V. Skryabin, and A. Vladimirov, Modulational instability of discrete solitons in coupled waveguides with group velocity dispersion, Opt. Express **14**, 12347 (2006).

[5] I. Babushkin, A. Husakou, J. Herrmann, and Y. S. Kivshar, Frequency-selective self-trapping and supercontinuum generation in arrays of coupled nonlinear waveguides, Opt. Express **15**, 11978 (2007).

[6] A. Joushaghani, R. Iyer, J. K. S. Poon, J. S. Aitchison, C. M. de Sterke, J. Wan, and M. M. Dignam, Quasi-Bloch Oscillations in Curved Coupled Optical Waveguides, Phys. Rev. Lett. **103**, 143903 (2009).

[7] Y. Lahini, E. Frumker, Y. Silberberg, S. Droulias, K. Hizanidis, R. Morandotti, and D. N. Christodoulides, Discrete X-Wave Formation in Nonlinear Waveguide Arrays, Phys. Rev. Lett. **98**, 023901 (2007).

[8] S. Longhi, Quantum-optical analogies using photonic structures, Laser and Photon. Rev. **3**, 243 (2009).

[9] S. Longhi, M. Marangoni, M. Lobino, R. Ramponi, P. Laporta, E. Cianci, and V. Foglietti, Observation of Dynamic Localization in Periodically Curved Waveguide Arrays, Phys. Rev. Lett. **96**, 243901 (2006).

[10] G. Lenz, I. Talanina, and C. M. de Sterke, Bloch Oscillations in an Array of Curved Optical Waveguides, Phys. Rev. Lett. **83**, 963 (1999).

[11] N. Chiodo, G. D. Valle, R. Osellame, S. Longhi, G. Cerullo, R. Ramponi, P. Laporta, and U. Morgner, Imaging of Bloch oscillations in erbium-doped curved waveguide arrays, Opt. Lett. **31**, 1651 (2006).

[12] R. El-Ganainy, K. G. Makris, D. N. Christodoulides, and Z. H. Musslimani, Theory of coupled optical PT-symmetric structures, Opt. Lett. **32**, 2632 (2007).

[13] N. K. Efremidis, Topological photonic Su-Schrieffer-Heeger-type coupler, Phys. Rev. A **104**, 053531 (2021).

[14] N. Malkova, I. Hromada, X. Wang, G. Bryant, and Z. Chen, Observation of optical Shockley-like surface states in photonic superlattices, Opt. Lett. **34**, 1633 (2009).

[15] J. T. Young, C. Wei, C. R. Menyuk, and J. Hu, Mode coupling at avoided crossings in slab waveguides with comparison to optical fibers: Tutorial, J. Opt. Soc. Am. B **38**, F104 (2021).

[16] Y. Liu, C. Wu, X. Qiang, J. Wu, X. Yang, and P. Xu, Evanescent-wave coupling phase-matching for ultrawidely tunable frequency conversion in silicon-waveguide chips, Opt. Express **27**, 28866 (2019).

[17] B. Liu, H. Yu, Z. Yuan Li, and L. Tong, Phase-matched second-harmonic generation in coupled nonlinear optical waveguides, J. Opt. Soc. Am. B **36**, 2650 (2019).

[18] A. Hardy and W. Streifer, Coupled mode theory of parallel waveguides, J. Lightwave Technol. **3**, 1135 (1985).

[19] H. Haus, W. Huang, S. Kawakami, and N. Whitaker, Coupled-mode theory of optical waveguides, J. Lightwave Technol. **5**, 16 (1987).

[20] J. Ding, J. Lin, and Y. Sun, Calculation of coupling length for spatial waveguides using planar waveguides, Optik **126**, 4319 (2015).

[21] M. Kuznetsov, Expressions for the coupling coefficient of a rectangular-waveguide directional coupler, Opt. Lett. **8**, 499 (1983).

[22] S. Kim, K. Han, C. Wang, J. A. Jaramillo-Villegas, X. Xue, C. Bao, Y. Xuan, D. E. Leaird, A. M. Weiner, and M. Qi, Dispersion engineering and frequency comb generation in thin silicon nitride concentric microresonators, Nat. Commun. **8**, 372 (2017).

[23] N. Kohli, S. Srivastava, and E. K. Sharma, Orthogonal solutions for asymmetric strongly coupled waveguide arrays: An elegant, analytical approach, J. Opt. Soc. Am. B **31**, 2871 (2014).

[24] S. G. Johnson, M. Ibanescu, M. A. Skorobogatiy, O. Weisberg, J. D. Joannopoulos, and Y. Fink, Perturbation theory for Maxwell's equations with shifting material boundaries, Phys. Rev. E **65**, 066611 (2002).

[25] M. Skorobogatiy, M. Ibanescu, S. G. Johnson, O. Weisberg, T. D. Engeness, M. Soljačić, S. A. Jacobs, and Y. Fink, Analysis of general geometric scaling perturbations in a transmitting waveguide: Fundamental connection between polarization-mode dispersion and group-velocity dispersion, J. Opt. Soc. Am. B **19**, 2867 (2002).

[26] M. Skorobogatiy, S. Jacobs, S. Johnson, and Y. Fink, Geometric variations in high index-contrast waveguides, coupled mode theory in curvilinear coordinates, Opt. Express **10**, 1227 (2002).

[27] E. Marcatili, Improved coupled-mode equations for dielectric guides, IEEE J. Quantum Electron. **22**, 988 (1986).

[28] S. Ghadirli, K. Thyagarajan, and A. Kumar, Band stop filter characteristics of non identical waveguides directional couplers; A comparison of three methods, Opt. Commun. **84**, 144 (1991).

[29] K. Okamoto, Coupled mode theory, in *Fundamentals of Optical Waveguides* (Elsevier, New York, 2006), pp. 159–207.

[30] P.-R. Loh, A. F. Oskooi, M. Ibanescu, M. Skorobogatiy, and S. G. Johnson, Fundamental relation between phase and group velocity, and application to the failure of perfectly matched layers in backward-wave structures, Phys. Rev. E **79**, 065601(R) (2009).

[31] X. C. Tong, Silicon-on-insulator waveguides, in *Advanced Materials for Integrated Optical Waveguides* (Springer International Publishing, Cham, 2013), pp. 253–287.

[32] H. Yıldırım, Dispersion parameters and nonlinear optical properties of silicon nitride rib waveguides, Opt. Commun. **284**, 2031 (2011).

[33] J. Wang, Z. Yao, and A. W. Poon, Silicon-nitride-based integrated optofluidic biochemical sensors using a coupled-resonator optical waveguide, Front. Mater. **2** (2015), doi: 10.3389/fmats.2015.00034.

[34] K. Hammani, L. Markey, M. Lamy, B. Kibler, J. Arocas, J. Fatome, A. Dereux, J.-C. Weeber, and C. Finot, Octave spanning supercontinuum in titanium dioxide waveguides, Appl. Sci. **8**, 543 (2018).

[35] J.-C. Weeber, K. Hammani, G. C. des Francs, A. Bouhelier, J. Arocas, A. Kumar, F. Eloi, S. Buil, X. Quélin, J.-P. Hermier, M. Nasilowski, and B. Dubertret, Colloidal quantum dot integrated light sources for plasmon mediated photonic waveguide excitation, ACS Photonics **3**, 844 (2016).

[36] M. Belt, M. L. Davenport, J. E. Bowers, and D. J. Blumenthal, Ultra-low-loss Ta_2O_5-core/SiO_2-clad planar waveguides on Si substrates, Optica **4**, 532 (2017).

[37] S. G. Johnsonand J. D. Joannopoulos, Block-iterative frequency-domain methods for Maxwell's equations in a planewave basis, Opt. Express **8**, 173 (2001).

[38] A. W. Snyderand J. D. Love, Green's function methods, in *Optical Waveguide Theory* (Springer, New York, 1983), pp. 656–665.

[39] L. Ramunnoand S. Hughes, Disorder-induced resonance shifts in high-index-contrast photonic crystal nanocavities, Phys. Rev. B **79**, 161303(R) (2009).

[40] A. Yaghjian, Electric dyadic greens functions in the source region, Proc. IEEE **68**, 248 (1980).

[41] O. J. F. Martinand N. B. Piller, Electromagnetic scattering in polarizable backgrounds, Phys. Rev. E **58**, 3909 (1998).

[42] S. G. Johnson, M. L. Povinelli, M. Soljačić, A. Karalis, S. Jacobs, and J. D. Joannopoulos, Roughness losses and volume-current methods in photonic-crystal waveguides, Appl. Phys. B **81**, 283 (2005).

[43] P. V. Rysselberghe, Remarks concerning the Clausius-Mossotti law, J. Phys. Chem. **36**, 1152 (1932).

[44] C. Böttcher, *Theory of Electric Polarization* (Elsevier, New York, 1973).

[45] V. A. Markel, Introduction to the Maxwell Garnett approximation: Tutorial, J. Opt. Soc. Am. A **33**, 1244 (2016).

[46] M. B. Doost, W. Langbein, and E. A. Muljarov, Resonant state expansion applied to two-dimensional open optical systems, Phys. Rev. A **87**, 043827 (2013).

[47] S. V. Lobanov, W. Langbein, and E. A. Muljarov, Resonant-state expansion applied to three-dimensional open optical systems: Complete set of static modes, Phys. Rev. A **100**, 063811 (2019).

[48] J. E. Sipe, Vector *k-p* approach for photonic band structures, Phys. Rev. E **62**, 5672 (2000).

[49] P. Y. Chen, D. J. Bergman, and Y. Sivan, Generalizing Normal Mode Expansion of Electromagnetic Green's Tensor to Open Systems, Phys. Rev. Appl. **11**, 044018 (2019).

[50] S. Rao, G. L. Saux, Y. Sivan, and P. Y. Chen, Generalized normal mode expansion method for open and lossy periodic structures, J. Opt. Soc. Am. B **39**, 1338 (2022).

[51] P. T. Kristensen, J. R. de Lasson, and N. Gregersen, Calculation, normalization, and perturbation of quasinormal modes in coupled cavity-waveguide systems, Opt. Lett. **39**, 6359 (2014).

[52] M. L. Cooper and S. Mookherjea, Numerically-assisted coupled-mode theory for silicon waveguide couplers and arrayed waveguides, Opt. Express **17**, 1583 (2009).

[53] M. Pattersonand S. Hughes, Interplay between disorder-induced scattering and local field effects in photonic crystal waveguides, Phys. Rev. B **81**, 245321 (2010).

[54] N. Mann, A. Javadi, P. D. García, P. Lodahl, and S. Hughes, Theory and experiments of disorder-induced resonance shifts and mode-edge broadening in deliberately disordered photonic crystal waveguides, Phys. Rev. A **92**, 023849 (2015).

[55] V. LeBihan, A. Pillonnet, D. Amans, G. Ledoux, O. Marty, and C. Dujardin, Critical dimension where the macroscopic definition of refractive index can be applied at a nanometric scale, Phys. Rev. B **78**, 113405 (2008).

[56] P. Lunnemann and A. F. Koenderink, The local density of optical states of a metasurface, Sci. Rep. **6**, 20655 (2016).

[57] M. Patterson, S. Hughes, D. Dalacu, and R. L. Williams, Broadband Purcell factor enhancements in photonic-crystal ridge waveguides, Phys. Rev. B **80**, 125307 (2009).

[58] M. Eguchi, Multilayered effective-index analysis of dielectric waveguides with complicated microstructures, J. Opt. Soc. Am. B **28**, 2478 (2011).

[59] N. Mann, S. Combrié, P. Colman, M. Patterson, A. D. Rossi, and S. Hughes, Reducing disorder-induced losses for slow light photonic crystal waveguides through Bloch mode engineering, Opt. Lett. **38**, 4244 (2013).

[60] K. S. Chiang, Performance of the effective-index method for the analysis of dielectric waveguides, Opt. Lett. **16**, 714 (1991).

[61] T. A. van der Sijs, O. El Gawhary, and H. P. Urbach, Electromagnetic scattering beyond the weak regime: Solving the problem of divergent Born perturbation series by Padé approximants, Phys. Rev. Res. **2**, 013308 (2020).

[62] O. J. F. Martin, A. Dereux, and C. Girard, Iterative scheme for computing exactly the total field propagating in dielectric structures of arbitrary shape, J. Opt. Soc. Am. A **11**, 1073 (1994).

[63] A. Udupiand S. K. Madhava, Plasmonic coupler and multiplexer/demultiplexer based on nano-groove-arrays, Plasmonics **16**, 1685 (2021).

[64] P. Lalanne, C. Sauvan, J. P. Hugonin, J. C. Rodier, and P. Chavel, Perturbative approach for surface plasmon effects on flat interfaces periodically corrugated by subwavelength apertures, Phys. Rev. B **68**, 125404 (2003).

[65] P. Lalanne, W. Yan, K. Vynck, C. Sauvan, and J.-P. Hugonin, Light interaction with photonic and plasmonic resonances, Laser Photonics Rev. **12**, 1700113 (2018).

[66] C. Sauvan, J. P. Hugonin, I. S. Maksymov, and P. Lalanne, Theory of the Spontaneous Optical Emission of Nanosize Photonic and Plasmon Resonators, Phys. Rev. Lett. **110**, 237401 (2013).

[67] M. B. Mia, S. Z. Ahmed, I. Ahmed, Y. J. Lee, M. Qi, and S. Kim, Exceptional coupling in photonic anisotropic metamaterials for extremely low waveguide crosstalk, Optica **7**, 881 (2020).

[68] L. C. Andreaniand D. Gerace, Photonic-crystal slabs with a triangular lattice of triangular holes investigated using a guided-mode expansion method, Phys. Rev. B **73**, 235114 (2006).

[69] J. Jensenand O. Sigmund, Topology optimization for nano-photonics, Laser Photon. Rev. **5**, 308 (2011).